6

Formation of Ultrahigh Density Quantum Dots Epitaxially Grown on Si Substrates Using Ultrathin SiO_2 Film Technique

Yoshiaki Nakamura[1] and Masakazu Ichikawa[2]
[1]*Graduate School of Engineering Science, Osaka University*
[2]*Department of Applied Physics, The University of Tokyo*
Japan

1. Introduction

Development of Si-based light emitter has been eagerly anticipated in Si photonics. However, its realization is difficult because group IV semiconductors such as Si and Ge are indirect-transition semiconductors. Si or Ge quantum dots (QDs) on Si substrates have drawn much attention as Si-based light emitting materials because their optical transition probability can be enhanced by their quantum confinement effect. There are some kinds of QDs fabricated by various methods: Stranski Krastanov (SK) QDs (Eaglesham & Cerullo, 1990; Schmidt & Eberl, 2000), Ge nanoparticles in SiO_2 matrix (Maeda, 1995), Si QDs by anodic oxidation (porous Si) (Wolkin et al., 1999; Cullis & Canham, 1991), and so on. In terms of the crystal orientation control, SK QDs have intensively attracted much interest. In general, the density of SK QDs is approximately $10^{10\text{-}11}$ cm^{-2} and the size is about 50-100 nm. In order to get strong light emission and quantum confinement effect, the higher density and smaller size are required.

We have developed a formation method of QDs using the ultrathin SiO_2 films which we call as ultrathin SiO_2 film technique (Shklyaev et al., 2000; Shklyaev & Ichikawa, 2001; Nakamura et al., 2004). In this method, Si or Ge QDs with ultrahigh density (>10^{12} cm^{-2}) and small size (<5 nm) were epitaxially grown on Si substrates, where lattice mismatch strain was not used for the formation of QDs unlike SK QDs. Furthermore, QDs were elastically strain-relaxed without misfit dislocations (Nakamura et al., 2010, Nakamura et al, 2011b). These high crystal quality ultrasmall QDs on Si can be expected as Si-based light emitting materials.

In order to use QDs on Si substrates as light emitter in Si photonics, the light wavelength corresponding to energy bandgap E_g has to be consistent with that for optical fiber communications: namely 1.3 μm (~0.95eV) or 1.5 μm (~0.8 eV) wavelength bands. Ge bulk has E_g of 0.67 eV at room temperature, but E_g of Ge QDs increases up to 1-1.5 eV at QD diameter of around 5 nm due to quantum confinement effect (Niquet et a.l, 2000; Nakamura et al, 2005). On the other hand, $Ge_{1-x}Sn_x$ alloy films have been reported to be direct-transition semiconductors (Jenkins & Dow, 1987; He & Atwater, 1997) at larger Sn content x

(x>~0.12) indicating the possibility of high light emitting efficiency. In terms of energy bandgap, however, it is much smaller (0.3–0.5 eV) at x of ~0.12 (de Guevara et al., 2004) than that for optical fiber communications. We noticed a possibility that the energy bandgap of the direct-transition semiconductor $Ge_{1-x}Sn_x$ QDs could increase up to ~0.8 eV using their quantum confinement effect.

The growth of $Ge_{1-x}Sn_x$ alloys is complicated by a limited mutual solid solubility of Ge and Sn (~1%), and a tendency for Sn surface segregation. Moreover, the epitaxial growth of high crystal quality $Ge_{1-x}Sn_x$ alloys on Si is difficult because of the large lattice mismatch between $Ge_{1-x}Sn_x$ alloys (x >~0.12) and Si. Development of formation technique of $Ge_{1-x}Sn_x$ QDs was required. In this chapter, we try to solve the above problems in $Ge_{1-x}Sn_x$ QD formation by modifying our ultrathin SiO_2 film technique and develop the epitaxial growth technique of ultrahigh density (>10^{12} cm^{-2}) $Ge_{1-x}Sn_x$ QDs at high Sn content (x>~0.1), where QDs have almost no misfit dislocation and ultrasmall size causing quantum confinement effect. We present the results of formation and physical properties of QDs epitaxially grown on Si

2. The formation technique of Si and Ge QDs using ultrathin SiO_2 films

We have developed the formation technique of QDs using ultrathin SiO_2 films (Shklyaev et al., 2000; Shklyaev & Ichikawa, 2001; Nakamura et al., 2004). Si or Ge deposition on the ultrathin SiO_2 films brings epitaxial growth of ultrasmall QDs with ultrahigh density (>10^{12} cm^{-2}). This growth mode is totally different from the conventional SK and Volmer Weber modes. At first, we introduce the details of this ultrathin SiO_2 film technique.

2.1 Ultrathin SiO_2 film technique for Ge and Si QD formation

Si(111) or Si(001) substrates were introduced into an ultrahigh vacuum chamber at the base pressure of ~1×10^{-8} Pa. Clean Si surfaces were obtained by flashing at 1250°C or by forming Si buffer layers. The clean Si surfaces were oxidized at ~ 600°C for 10 min at the oxygen pressure of 2×10^{-4} Pa to form ultrathin SiO_2 films (<1 nm) (Matsudo et al., 2002). Then, Si or Ge was deposited on the ultrathin SiO_2 films at 500°C using an electron beam evaporator or a Knudsen cell to form spherical Si or Ge QDs with an ultrahigh density of ~ 2×10^{12} cm^{-2}. Scanning tunneling microscope (STM) experiments were conducted at the sample bias voltage of 3-6 V and tunnelling current of 0.2 nA at room temperature (RT) using sharp chemically treated W tips (Nakamura et al., 1999).

Figures 1(a) and (b) show STM image and reflection high energy diffraction (RHEED) pattern of the ultrathin SiO_2 film, respectively. STM image describes amorphous surface.

STM images of Si and Ge QDs were shown in Figs. 2(a) and 2(b), which were formed by deposition of 8-monolayer (ML) Si and 5-ML Ge, respectively, at 500°C. Spherical QDs of ~5 nm in diameter were grown on Si substrates with an ultrahigh density of ~ 2×10^{12} cm^{-2}. RHEED pattern revealed that at deposition temperature higher than ~450°C, QDs were epitaxially grown with the same crystal orientation of the Si substrates as shown in Figs. 2(c). On the other hand, at deposition temperature lower than ~400°C, RHEED of QDs exhibited Debye ring pattern indicating that QDs were non-epitaxially grown on Si substrates.

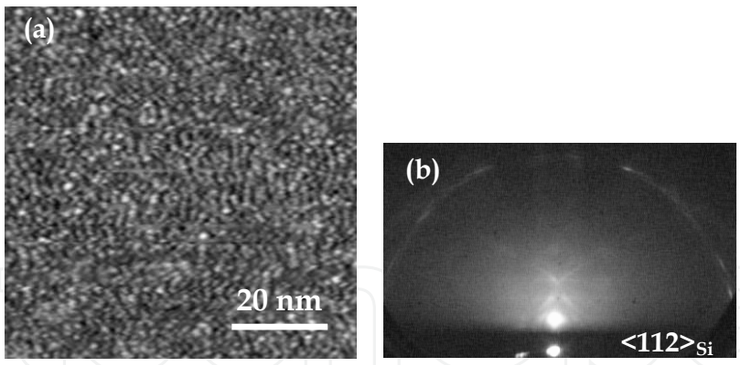

Fig. 1. (a) STM image and (b) RHEED pattern of ultrathin SiO_2 film on Si (111) substrate.

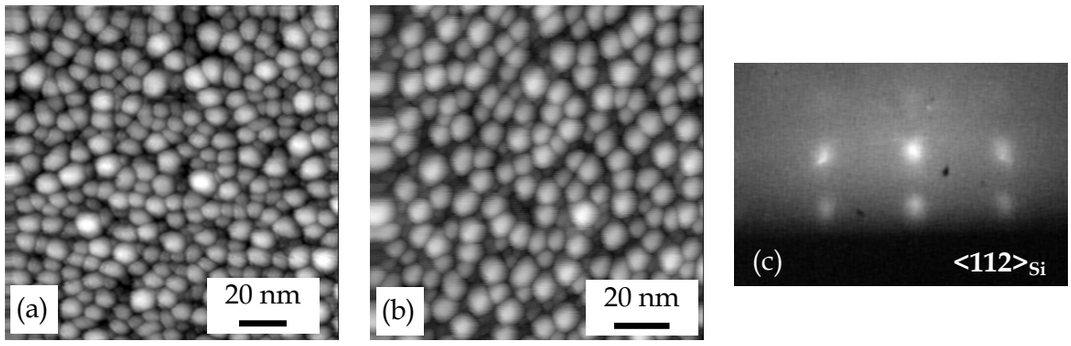

Fig. 2. STM images of Si (a) and Ge QDs (b) on Si (111) substrates formed by deposition of 8-ML Si and 5-ML Ge. (c) RHEED pattern of Ge QDs shown in (b).

2.2 Mechanism of ultrahigh density QD formation by ultrathin SiO_2 film technique

Mechanism of ultrahigh density QD formation (Shklyaev et al., 2000; Shklyaev & Ichikawa, 2001; Nakamura et al., 2004) is illustrated in Fig. 3. At the first stage of Si or Ge deposition on the ultrathin SiO_2 films, deposited atoms diffuse on the surfaces and react with the ultrathin SiO_2 films after certain lifetime, τ through the following reactions,

$$Si+SiO_2 \rightarrow 2SiO\uparrow, \text{ or } Ge+ SiO_2 \rightarrow SiO\uparrow+GeO\uparrow. \quad (1)$$

As a result, at reaction sites, the nanometer-sized windows (nanowindows) are formed in the ultrathin SiO_2 films. The distance between nanowindows is determined by diffusion length of deposited atoms until they react with the ultrathin SiO_2 films, $\sim\sqrt{D\tau}$, where D is the diffusion coefficient. In the case of Si and Ge, this value is approximately 10 nm resulting in the ultrahigh density (~10^{12} cm^{-2}). Nanowindows are functioned as trap sites for deposited atoms due to the dangling bonds. In other words, the chemical potential of deposited atoms at the nanowindow sites is smaller than that on the ultrathin SiO_2 film. Then, nanowindows work as nucleation sites for QD growth resulting in the formation of ultrahigh density spherical QDs. Despite the existence of the ultrathin SiO_2 films, epitaxial growth of our QDs is understood in this scenario as shown in Fig. 4. When the deposition temperature is high (>~450°C), nanowindows form sufficiently through reaction (1). As a

result, the formed QDs contact with Si substrates through nanowindows leading to the epitaxial growth. On the contrary, when the deposition temperature is low (<~400°C), nanowindows do not penetrated into Si substrates due to insufficiency of reaction (1), resulting in non-epitaxial growth of QDs. As for epitaxial QDs, the limited nanocontact between QDs and substrates reduces the strain energy in QDs induced by lattice mismatch. The QDs are elastically strain-relaxed without misfit dislocation due to the small strain energy and spherical shape. This unique formation mechanism brings high quality in QDs.

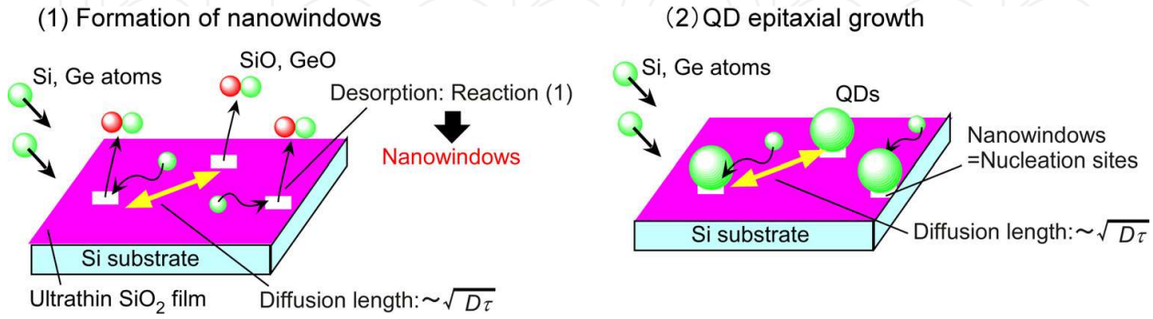

Fig. 3. Illustration of mechanism of ultrahigh density QD formation by ultrathin SiO_2 film technique.

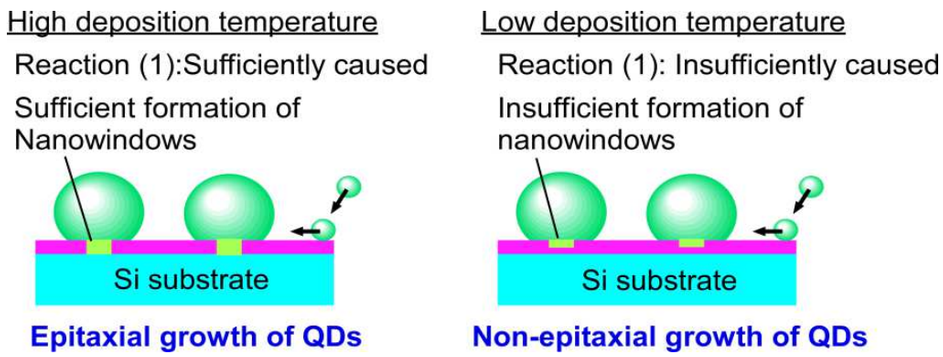

Fig. 4. Schematic of mechanism of epitaxial or non-epitaxial growth of QDs

3. Modified formation technique for QDs of other materials

To apply the aforementioned ultrathin SiO_2 film technique to materials other than Si and Ge, we modified this technique in the following way (Fig. 5) (Nakamura et al., 2006; Nakamura et al., 2009). First, ultrahigh density nanowindows were formed in the ultrathin SiO_2 films by predeposition of Si or Ge. Second, materials A and B were codeposited with flux ratio of 1-x to x to form epitaxial $A_{1-x}B_x$ QDs. In this proposed technique, there are several advantages: (1) Ultrahigh density QDs can be formed because ultrahigh density nanowinows work as nucleation sites. (2) QD size is controllable down to ~1 nm by controlling deposition amount. (3) Tuning flux ratio enables the composition control. (4) Existence of nanowindows allows the epitaxial growth on SiO_2 films. (5) The SiO_2 films prevent diffusion of deposited atoms into Si substrates. (6) The technique can be applied to various materials. (7) Limited contact between QDs and Si substrates enables elastic strain-relaxation in spherical QDs without introduction of misfit dislocation in their heterointerfaces (Nakamura et al., 2010; Nakamura et al, 2011a, Nakamura et al, 2011b).

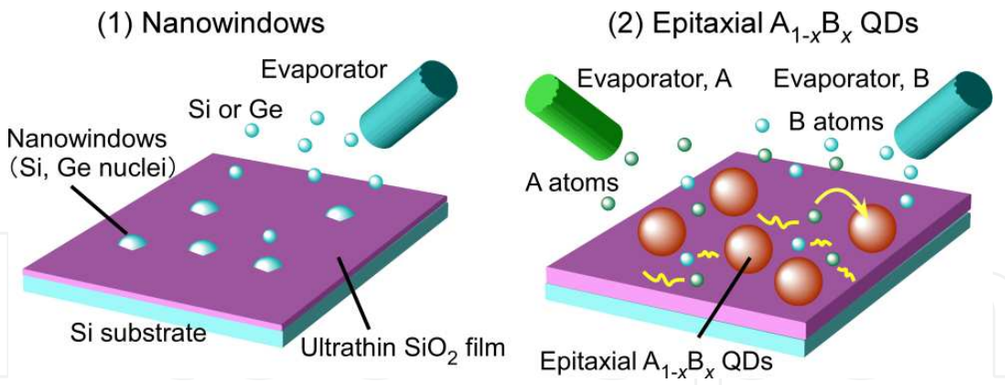

Fig. 5. Idea of the modified ultrathin SiO_2 film technique

Here, we focus on Ge_{1-x} Sn_x which were reported to be direct-transition semiconductor at larger x>~0.12 (Jenkins & Dow, 1987; He & Atwater, 1997). Based on the above idea, we have developed epitaxial growth technique of ultrahigh density Ge_{1-x} Sn_x QDs on Si substrates (Nakamura et al., 2007c) which is a promising material for light emitter. This ultrathin SiO_2 film technique and the physical properties of these QDs are presented.

3.1 Experimental procedure

Samples cut from Si(111) or Si(001) wafers were introduced into an ultrahigh-vacuum chamber with a base pressure of about 1×10^{-8} Pa. The chamber was equipped with a STM, a RHEED apparatus, and two separate Knudsen cells for Ge and Sn deposition. Ultrathin SiO_2 films with thicknesses of ~0.3 nm (Matsudo et al., 2002) were formed by oxidizing the Si surfaces in the chamber at 600°C for 10 min at an oxygen pressure of 2×10^{-4} Pa, after cleaning the Si surfaces by flashing at 1250°C. To form nanowindows in the ultrathin SiO_2 films, we deposited a small amount of Ge on the ultrathin SiO_2 films under various conditions, i.e. a Ge deposition amount of 1-2 ML at temperatures of 500-650°C, a process that is referred to as Ge predeposition. We considered that nanowindow formation by Ge predeposition was needed to initiate contact between the QDs and Si substrates through SiO_2 films to grow epitaxial QDs. The nanowindow formation mechanism has been reported in our papers (Shklyaev et al., 2000; Shklyaev & Ichikawa, 2001; Nakamura et al., 2004). Ge and Sn were codeposited on these ultrathin SiO_2 films with nanowindows at ~100-200°C at the flux ratio of 1-x to x to form $Ge_{1-x}Sn_x$ QDs. This low temperature growth of ~100-200°C was required for the growth of the supersaturated GeSn alloy films (He & Atwater, 1997.; Gurdal et al., 1998, Ragan & Atwater, 2000., de Guevara et al., 2003). Sn atoms might segregate in the samples with large Sn content x, but in the present chapter, the Sn content x in the QDs was described as flux ratio. RHEED patterns were observed using a 15-keV electron beam with an incident direction of $<112>_{Si}$ for Si(111) substrates and $<110>_{Si}$ for Si(001) substrates. Typical STM experiments were conducted at a sample bias voltage, V_S of +2-5 V and a tunneling current, I_T of 0.1 nA at room temperature using chemically-sharpened W tips (Nakamura et al., 1999). STS experiments were performed at V_S of +0.8 V and at I_T of 0.1 nA at RT using chemically-polished PtIr tips cleaned by electron beam heating in UHV chamber. Before STS measurements, in order to remove the surface state contribution in the energy bandgap, we performed atomic hydrogen termination of the QD surfaces by introducing hydrogen molecules up to 2×10^{-4} Pa for 70 min at room temperature after putting the samples in front of heated W filaments. When we observed cross section of

the samples using ex-situ high-resolution transmission electron microscopy (HRTEM) and scanning transmission electron microscopy (STEM), the samples were covered with amorphous 20-ML Si films.

3.2 Formation of GeSn QDs using ultrathin SiO_2 film technique

Figures 6(a) and (b) are STM image and RHEED pattern of the ultrathin SiO_2 film on Si(111) substrates, respectively, where nanowindows were formed by Ge predeposition in 2-ML amounts at 650°C. The STM results revealed that Ge predeposition formed Ge nuclei on the SiO_2 films. At the first stage of Ge predeposition, voids were formed in the ultrathin SiO_2 films through reaction (1), and the extra atoms of deposited Ge were trapped at the void sites resulting in the formation of Ge nuclei. We call the Ge nuclei on voids as nanowindows in this case. Ge nuclei has ultrasmall volume due to the volatilization of GeO. Obscure 1×1 diffraction patterns in Fig. 6(b) indicates that the Ge nuclei were crystals epitaxially grown on the substrates through the voids, with the same crystallographic orientations as those of the substrates.

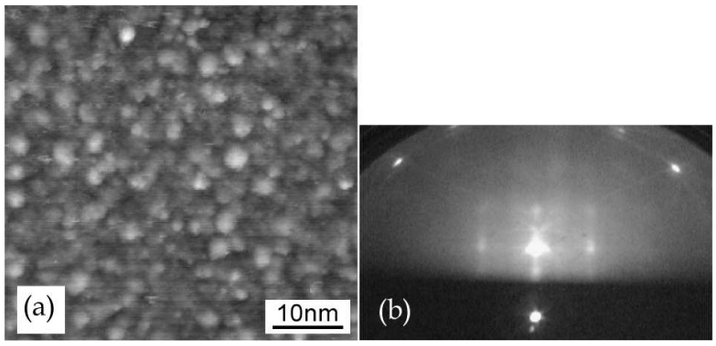

Fig. 6. (a) STM image and (b) RHEED pattern of the ultrathin SiO_2 films with predeposited Ge in 2-ML amounts at temperatures of 650°C.

After the nanowindows were formed on the ultrathin SiO_2 films by 2-ML Ge deposition at 650°C, we codeposited Ge and Sn at 200°C to form $Ge_{0.85}Sn_{0.15}$ QDs as shown in Fig. 7(a). In order to prevent Sn segragation, codeposition temperature should be less than ~200°C . Spherical $Ge_{0.85}Sn_{0.15}$ QDs of ~5 nm in diameter were formed with an ultrahigh density (~2×10^{12} cm^{-2}). RHEED pattern of this sample shows the diffraction pattern revealing the epitaxial growth of QDs with the same orientation as that of Si substrates.

Morphorlogy of $Ge_{0.85}Sn_{0.15}$ QDs was independent of predeposition condition for the nanowindow formation. However, the crystal orientation relationships between QDs and substrates strongly depended on the predeposition condition. We closely observed RHEED patterns of $Ge_{0.85}Sn_{0.15}$ QDs codeposited at 100°C, where the nanowindows were formed under various predeposition conditions. In the case of low predepositoin temperature of 500°C, Debye rings appeared in RHEED patterns demonstrating non-epitaxial growth of QDs as shown in Fig. 7(c), regardless of the amount of predeposited Ge amout (1-2 ML). On the other hand, in the case of high predeposition temperature of 650°C, epitaxial spots were observed in the RHEED patterns as shown in Fig. 7(b). However, for small amounts of Ge predeposition (1 ML), Debye rings were also observed, albeit only slightly, in addition to the spot patterns. Epitaxial spots without Debye rings

appeared only in the case of 2-ML Ge predeposition, indicating that the $Ge_{1-x}Sn_x$ QDs were epitaxially grown only if 2-ML Ge was predeposited on the ultrathin SiO_2 films at 650°C for nanowindow formation. The predeposition condition is essential for epitaxial growth of QDs. For Si(001) substrates, the formation of $Ge_{1-x}Sn_x$ QDs using the same methods was confirmed, indicating that this formation technique does not depend on the face orientations of substrates.

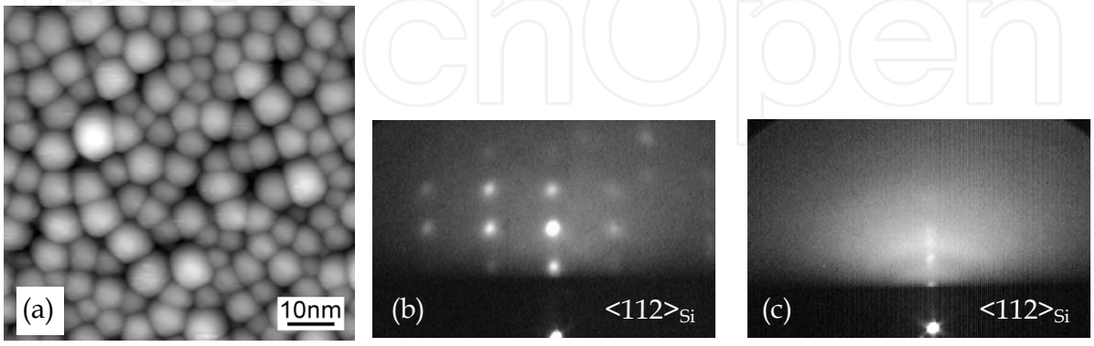

Fig. 7. (a) STM image of 8-ML $Ge_{0.85}Sn_{0.15}$ QDs formed by codeposition of Ge and Sn at 200°C on the ultrathin SiO_2 films with nanowindows. (b, c) RHEED pattern of 8-ML $Ge_{0.85}Sn_{0.15}$ QDs fomred by codeposition at 100°C. 2ML Ge was predeposited on the ultrathin SiO_2 films at 650 (a, b) and 500° C (c).

Reaction (1) occurred only during the Ge predeposition stage and not during the codeposition, because the codeposition temperatures (~100-200°C) were lower than that needed for reaction (1) (>~400°C) (Shklyaev et al., 2000). Excessive Ge atoms, which were not consumed by reaction (1) during predeposition, were used for epitaxial growth of Ge nuclei on the ultrahigh density voids resulting in the formation of ultrahigh density nanowindows, the mechanism of which is the same as that for ultrahigh density Ge QD formation (Shklyaev et al., 2000). The nanowindows worked as nucleation sites for $Ge_{1-x}Sn_x$ QD formation during codeposition, resulting in the epitaxial growth of ultrahigh density QDs. Under other predeposition conditions, (namely Ge amounts less than 2 ML or temperatures less than 650°C), the non-epitaxial growth of $Ge_{1-x}Sn_x$ QDs revealed the insufficiency of reaction (1). Increases in the amount of predeposited Ge or predeposition temperature can cause sufficient nanowindow formation. However, an excessive increase in the amount of predeposited Ge causes the Sn content, x in $Ge_{1-x}Sn_x$, to deviate from the objective value of ~0.15. Furthermore, a substrate temperature larger than 700°C causes the decomposition of SiO_2 films. Therefore, the Ge nucleus formation condition, a key factor for the epitaxial growth of $Ge_{1-x}Sn_x$ QDs, is limited.

The $Ge_{1-x}Sn_x$ QDs were annealed at 500°C for 3 min to improve low crystallinity of low-temperature-grown QDs (200°C). Althogh this annealing process caused only a slight increase in the QD diameter and a slight decrease in the QD density by QD coalescence, QD size and diameter are still similar to those of non-annealed QDs, namely, nanometer-size and ultrahigh density (~10^{12} cm^{-2}). Then, we used this condition for formation of epitaxial $Ge_{1-x}Sn_x$ QDs: predeposition of 2-ML Ge at 650°C, codepositon of Ge and Sn at 200°C, and annealing at 500°C for 3 min. We refer to this condtion as the epitaxial QD

growth condition. Figure 8(a) shows a cross-sectional HRTEM image of the 8-ML epitaxial $Ge_{0.85}Sn_{0.15}$ QDs on Si(111). The QDs were fabricated under the above epitaxial QD growth condition. Spherical $Ge_{0.85}Sn_{0.15}$ QDs were formed with clear interfaces on the Si surfaces. The diameter and height of the QDs are ~7 and ~3 nm, respectively. These values were more precise than values measured in the STM images owing to STM tip apex effect. An FFT pattern of the $Ge_{0.85}Sn_{0.15}$ QD area shows a diffraction pattern corresponding to the epitaxial growth on Si(111). An inverse fast Fourier transform (IFFT) was performed through the $1\bar{1}0$ spots in the FFT pattern corresponding with the dashed square area in Fig. 8(a), where the area included the interface between the $Ge_{085}Sn_{0.15}$ QDs and Si substrate. The lattice planes were clearly shown in IFFT image in Fig. 8(b). No differences were found between the numbers of atomic planes on the sides of Si substrates and of QDs near their interfaces in the IFFT images in Fig. 8(b), except for the line deformation. This indicated there were no misfit dislocations at the interfaces between QDs and Si substrates. Furthermore, the line spacing became larger in the upper part of the QD in Fig. 8(b) although the line spacing in the QD was almost the same as that of Si substrates at the interface. Therefore, we considered that some strain in the upper part of QDs relaxed due to the spherical shape of QDs, instead of the formation of misfit dislocation. Figure 8(c) is an STEM image of the same sample with the same electron incident direction used for the HRTEM observation, where it is possible to detect the atomic number difference as the contrast difference. No contrast difference was found within the QDs, indicating no Sn segregation in the QDs within the spatial resolution of this measurement. To estimate the lattice constant of the $Ge_{0.85}Sn_{0.15}$ QDs, the FFT patterns of the $Ge_{0.85}Sn_{0.15}$ QD areas were compared with those of perfect Si substrate areas far from the interface. The lattice constants of the QDs in the in-plane direction (a_i) and growth direction (a_g) were measured from $1\bar{1}0$ and 222 diffraction spots in FFT patterns. For the main $Ge_{0.85}Sn_{0.15}$ QDs, there is almost no difference between a_i and a_g within the experimental errors. This indicates that main QDs exhibit little or no strain. The lattice constants individually measured for these QDs were 0.575±0.03 nm. One might consider that less-strained QDs were grown by the formation of misfit dislocations. However, the HRTEM images exhibited no misfit dislocations in the QDs. This indicates that heteroepitaxial strain is relaxed elastically in spherical QDs due to their sperical shape. Originally, there are two reasons that the present QDs would have small strain energy even if QDs were not be elastically strain-relaxed. One is the ultrasmall QD volumes that can have only small strain emergy. The other is due to the small contact betwen QDs and substrates through nanowindows (~1nm) in the ultrathin SiO_2 films (Nakamura et al., 2007a. Nakamura et al., 2010) unlike the heteropetaixal films or Stranski-Krastanov islands. These nanowindows were difficult to observe in Fig. 8(a). The measured lattice constants of QDs with almost no strain (0.575±0.003 nm) are larger than those of Ge (0.565 nm), which is derived from the alloying of Ge and Sn, rather than from the strain effect in the heterostructures. According to reports on the strain-relieved $Ge_{1-x}Sn_x$ alloy films (He & Atwater, 1997; de Guevara et al., 2003), the lattice constant of the $Ge_{1-x}Sn_x$ QDs gave a Sn concent x of 0.1-0.13. The Sn content value was smaller than the Sn flux ratio of 0.15 used during codeposition. This can be explained by considering the existence of Ge nuclei formed by Ge predeposition. In the case of 8-ML $Ge_{1-x}Sn_x$ QDs, 6.8-ML Ge and 1.2-ML Sn were deposited during the codeposition process. Therefore, considering an amount of Ge nuclei less than 2 ML, the content x ranges from 0.12 to 0.15, which agreed approximately with

the experimental results. The HRTEM observation revealed that QDs were elastically strain-relaxed without misfit dislocations and that the Sn content in $Ge_{1-x}Sn_x$ alloy is close to 0.15. This high x value and high crystal quality can be achieved only in the present QDs. The high x value in our $Ge_{1-x}Sn_x$ QDs is found to be astounding by comparing with that of reported $Ge_{1-x}Sn_x$ alloy films. This may be due to the aforementioned elastic strain-relaxation in nanometer-sized spherical QDs.

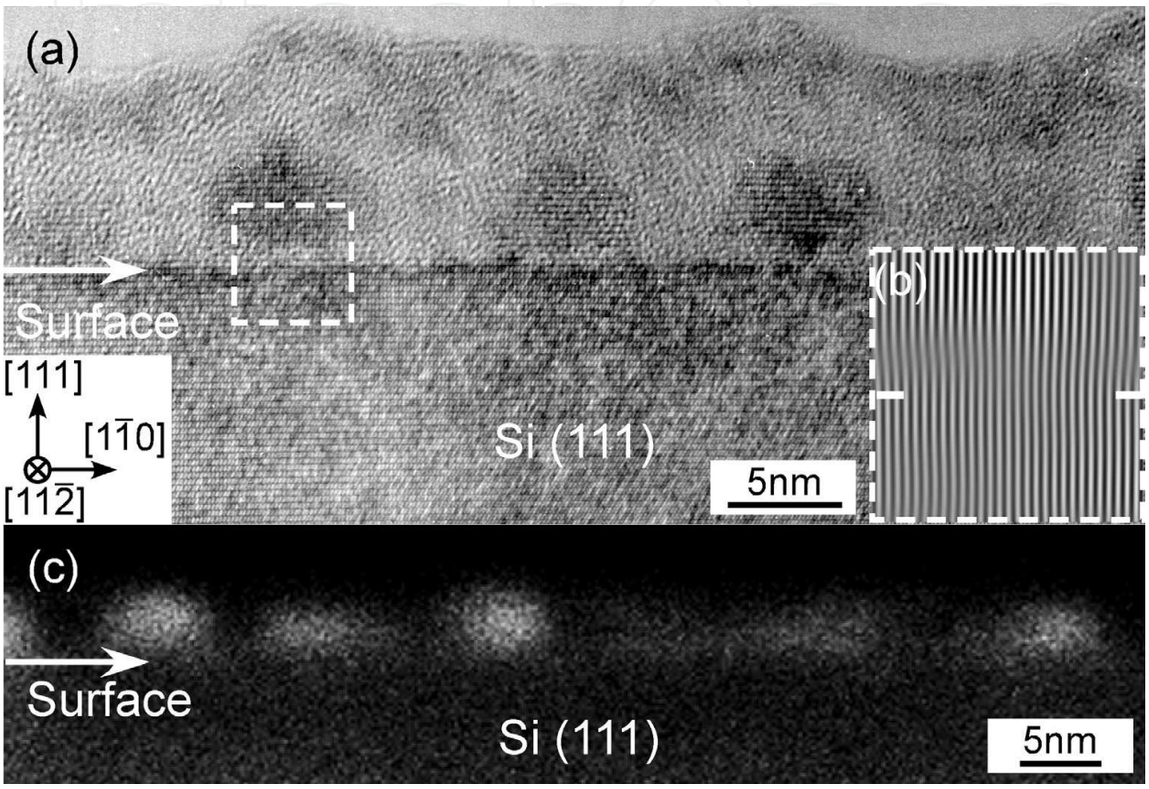

Fig. 8. (a) Cross sectional HRTEM image and (c) STEM image of epitaxial 8-ML $Ge_{0.85}Sn_{0.15}$ QDs on Si(111) formed under the epitaxial QD growth condition. (b) IFFT image of dotted squre area in (a). Two white lines in (b) indicat interface between QDs and substrate.

3.3 Electronic properties

We investigated electronic sates of $Ge_{1-x}Sn_x$ QDs individually using STS measurement (Nakamura et al., 2007b.). The QDs we measured are prepared by the hydrogen-termination of epitaxial $Ge_{0.85}Sn_{15}$ QDs formed under the epitaxial QD growth condition. The differential conductances, dI/dV, in Figs. 9(d)-(f) were obtained by STS measurements on the top of the hydrogen-terminated epitaxial $Ge_{0.85}Sn_{15}$ QDs indicated by the arrows in STM images in Figs. 9(a)-(c), respectively. Peaks in the conduction (p+) and valence (p-) band regions were observed in these spectra, though the p- peaks were sometimes not discernible. Difficulties of observing peaks in the valance band have been reported for other semiconductors (Grandidier, 2004). Figure 9 demonstrates that the p+ peak up-shifted with the decrease in the QD size. We also found various peak shapes, sharp and step-like peaks, as shown in Figs. 9(d) and (f). The peaks were broader for flattened QDs than those for spherical QDs.

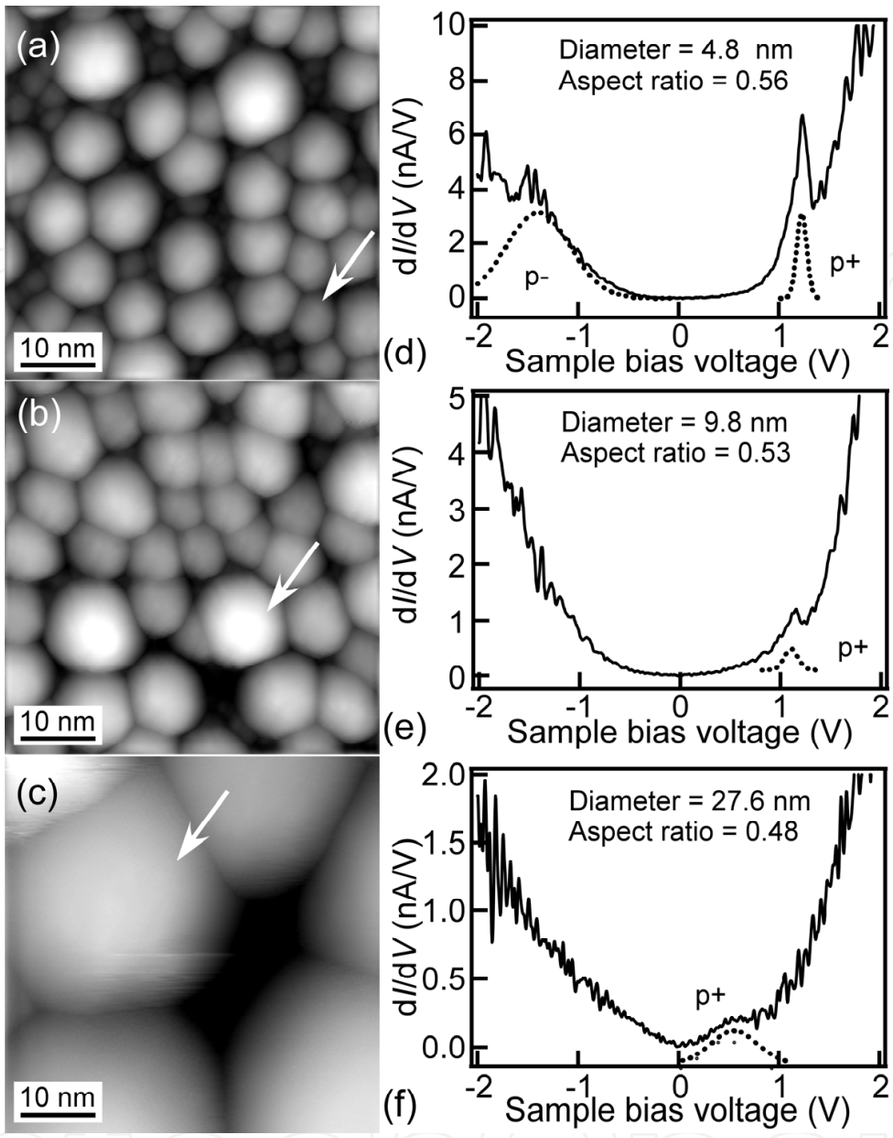

Fig. 9. (a), (b), (c) STM images of annealed $Ge_{0.85}Sn_{0.15}$ QDs with various deposition amount of 4-24 ML. (d), (e), (f) STS results corresponding to QDs indicated by arrows in (a), (b) and (f), respectively.

We measured the peak position and its width by deconvolution of the spectra using Gaussian functions with a standard deviation, σ as shown by dashed lines in Figs. 9 (d)-(f). We defined the CBM (VBM) by subtracting (adding) 2σ from (to) the peak position of p+ (p-). Figure 10(a) show the dependences of CBM and VBM on the diameter, *d* of the QDs. It is clear that the absolute values of both VBM and CBM up-shifted by about 0.5 eV with the decrease in the QD diameter from 35 to 4 nm. The QD-diameter dependence of the energy bandgap, defined as CBM-VBM, is shown in Fig. 10(b). The energy bandgap increased with a decrease in QD size. An interesting thing is the origin of the peaks in the STS spectra for the QDs. The peaks in the region of the energy bandgap may originate from the surface states. In the present case, however, we measured the hydrogen-terminated QDs, where the surface states were removed

in the region of the energy bandgap (Boland, 1991). Moreover, the peak positions shifted depending on the QD size. These results ruled out the possibility that the peaks originated from the surface states. Therefore, we considered that the peaks corresponded with the quantum levels derived from the quantum-confinement effect in the $Ge_{1-x}Sn_x$ QDs.

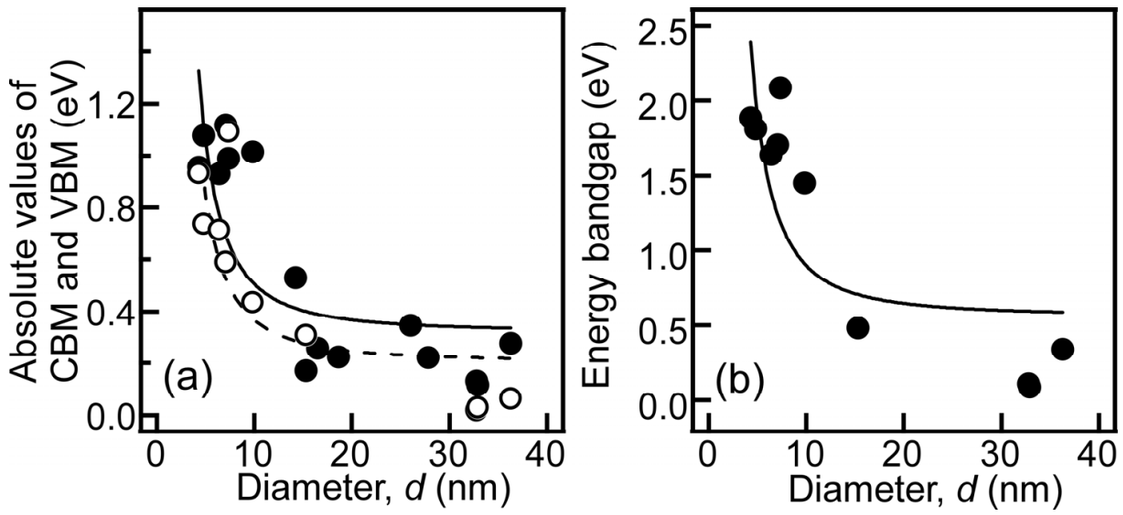

Fig. 10. (a) CBM (circles) and VBM (cricles) estimated from STS results of $Ge_{0.85}Sn_{0.15}$ QDs. (b) Energy bandgap calculated from CBM -VBM .

We investigated the dependence of the peak width of p+, defined as 2σ on the QD aspect ratio (=height to diameter). Figure 11(a) shows the strong dependence of the peak width on the QD aspect ratio. The peaks became broader as the QDs changed from spherical to flat ones (quantum well for an extremely small aspect ratio). In general, the density of states (DOS) in QDs changes gradually as a function of the dimensions of the QD (Grandidier, 2004). As QDs become flattening, the DOS of QDs gradually changes from sharp peak

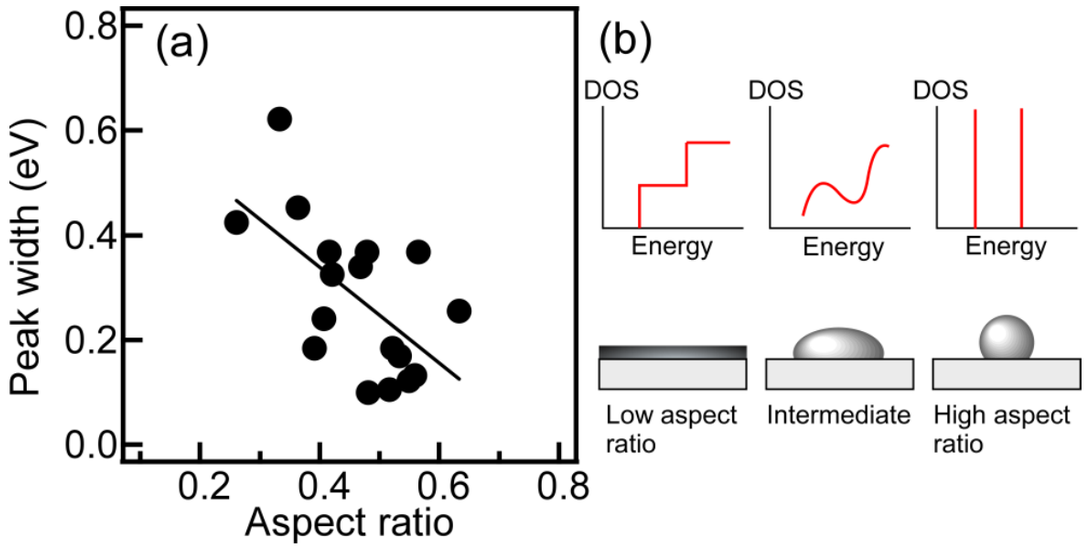

Fig. 11. (a) Dependence of peak width in STS on aspect ratio of QDs. (b) Illustration of density of states depending the QD shape.

structures for 0-dimensional (0-D) QDs to step-wise structures with electron and hole subbands for 2-D structures, through broad peak structures for states that are quasi-0-D QDs. As illustrated in Fig. 11(b), the dependence of the peak width on the QD aspect ratio can be explained by the gradual emergence of 2 dimensionality in DOS of quasi-0-D QDs as the QDs became flatter.

As mensioned in the 3.2 section, there were no differences between the lattice constants in in-plane and growth directions estimated by analysis of cross sectional HRTEM images, which indicated strain-free QDs (Nakamura et al., 2007c). Furthermore, STEM contrast in QDs was uniform. From these results, we considered that within this measurement accuracy, the present QDs were uniform in alloying and strain-free $Ge_{1-x}Sn_x$ QDs with x of 0.1-0.13. In the present situation, the strain-free QDs are sandwiched between vacuum and SiO_2 films. There are nanowindows between the SiO_2 films and the QDs, but they are ultrasmall (<~1nm), so that the carriers can hardly penetrate into the substrates (Nakamura et al., 2007a). The SiO_2 films work as the high barrier for the carriers in the QDs. Therefore, the hard wall square potential model is considered to be reasonable. For the quantum-confinement effect for QD diameter, d, the absolute value of CBM (VBM) for a confined structure, E_{confined} is described as

$$E_{\text{confined}}(d) = E_{\text{bulk}} + \frac{\hbar^2 \pi^2}{2\mu(d/2)^2} \tag{2}$$

where E_{bulk}, is the absolute value of CBM (VBM) for the bulk structure, and μ is the effective mass of the electron (hole). The solid (dashed) lines in Figs. 10(a) are best-fitted curves, where E_{bulk} for the absolute values of CBM (VBM) with respect to the Fermi level, and μ for the electron (hole) were adjusted to 0.32±0.09 eV (0.21±0.11 eV) and 0.080±0.018m_0 (0.092±0.026 m_0), respectively. The theoretical effective mass of an electron, m_e is reported to be ~0.1m_0 (Jenkins & Dow, 1987) and that of the hole is expected to be similar to the hole effective mass for Ge, m_h (~0.076 m_0) because the valence band structure near the Γ point is insensitive to the alloying of Ge and Sn (Jenkins & Dow, 1987). From the rough consistency between these values and the fitted μ values in Figs. 10(a), we found that our experimental result of the size dependence agreed with the quantum-confinement effect model for the 0-D QDs demonstrating that the present QDs were quasi-0-D structures.

The size dependence of energy bandgap due to the quantum-confinement effect can also be written by Eq. (2) when E_{bulk} and μ are the bulk energy bandgap and the reduced electron-hole mass, respectively, for $Ge_{1-x}Sn_x$ alloys. The solid line in Fig. 10(b) is a best-fitted curve with Eq. (2) where the E_{bulk} and μ were adjusted to 0.56±0.2 eV and 0.044±0.012m_0, respectively. This μ value agreed with the calculated one (~0.043 m_0) from m_e (~0.1 m_0) and m_h (~0.076 m_0). According to the relationship between energy bandgap and Sn content, x, for strain-relieved $Ge_{1-x}Sn_x$ alloys (He & Atwater, 1997; de Guevara et al., 2004), the energy bandgap was inferred as ~0.4-0.5 eV for x of 0.1-0.13. This value was roughly consistent with the fitted value E_{bulk} of 0.56±0.2 eV.

3.4 Optical properties

We formed Si capping layers on GeSn QDs by successive Si deposition at 400°C after 3 nm Si deposition at 200°C to fabricate the structures of Si/$Ge_{1-x}Sn_x$ QDs/Si(001). For PL

measurement of the Si/$Ge_{1-x}Sn_x$ QDs/Si(001) structures, we used a HeCd laser with a 325 nm wavelength and InGaAs photomultiplier detector. Figures 12(a) and (b) are STM image and RHEED pattern of the 40 nm Si capping layer formed on the $Ge_{0.85}Sn_{0.15}$ QDs epitaxially grown on Si (001) substrates that is Si/$Ge_{0.85}Sn_{0.15}$ QDs/Si . As mentioned in 3.2 section, spherical QDs were epitaxially grown on Si(001) with an ultrahigh density of ~10^{12} cm^{-2} under the epitaxial QD growth condition as is the case with Si (111) substrates. They show the epitaxial Si capping layer formed with the same crystallographic orientation as those of Si (001) substrates and of the underlying QDs and substrates.

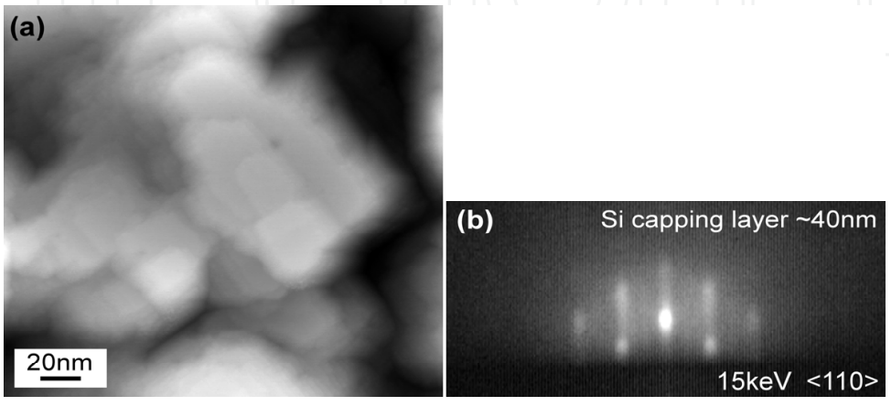

Fig. 12. (a) STM image and (b) RHEED pattern of Si/$Ge_{0.85}Sn_{0.15}$ QDs/Si(001) structure

To investigate the quantum size effect, we formed epitaxial $Ge_{0.85}Sn_{0.15}$ QDs with various QD diameters d (7, 9, and 13 nm) under the epitaxail QD growth condition by changing the deposition amounts (5, 8, and 14 ML) and covered these QDs with 60 nm Si capping layers. RHEED patterns of these Si capping layers indicated all Si capping layers were epitaxially grown. With a decrease in the size of the underlying QDs, the RHEED patterns become streakier, indicating the Si capping layer is becoming flatter. We measured PL spectra of these Si-capped $Ge_{0.85}Sn_{0.15}$ QDs with various QD sizes at 5 K as shown in Fig. 13. The PL peak appeared near 0.8 eV in all samples and the peak position was almost independent of the QD size indicating there was no quantum size effect. On the other hand, the PL intensity at the peak increased with a decrease in the QD size. The inset in Fig. 13 shows PL results of as-grown and post-annealed samples of the 60-nm-Si-capped Ge QD structures (dotted lines) that is Si/Ge QDs/Si sturcutres, for reference (Shklyaev et al., 2006.; Ichikawa et al., 2008). The inset shows these as-grown $Ge_{0.85}Sn_{0.15}$ QD samples have PL intensity about 10 times higher than that of as-grown Ge QD samples. The high intensity of these as-grown samples is comparable to that of the high-temperature-post-annealed Ge QD samples (900°C for 30 min).

The experimental result of the increase in the PL intensity with a decrease in QD size as shown in Fig. 13 is explained by two possible mechanisms. One is that these PL results come from the optical transition between the quantum levels in the QDs, where the oscillator strength is enhanced owing to the quantum confinement effect caused by the QD size decrease. The second is the reduction of the non-radiative recombination centers in the Si capping layer due to flatter Si capping layers with a decrease in the size of the underlying QDs. The experimental result with no quantum size effect in PL rules out the light emission mechanism from the QDs. In comparison with the similar PL of Si-capped Ge QDs

(Shklyaev et al., 2006; Shklyaev et al., 2007; Ichikawa et al., 2008), we consider the PL near ~1.5 μm of the present samples presumably originated from the radiative electronic states in the Si capping layers. This also reveals that the PL intensity enhancement due to the QD size decrease is caused by the latter mechanism; that is, the reduction of non-radiative recombination centers in the Si capping layer.

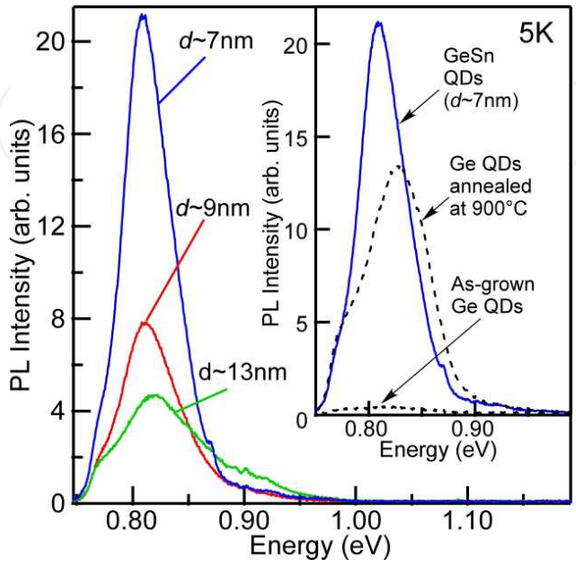

Fig. 13. PL spectra of Si/$Ge_{0.85}Sn_{0.15}$ QDs/Si(001) structures with QD diameter *d* of 7, 9 , and 13 nm. In inset, PL spectra of Si/Ge QDs/Si(001) structure before and after annealing at 900 are shown for reference.

To investigate the influence of Ge-Sn alloying in QDs on the high PL intensity, we measured the dependence of the PL spectrum on the Sn content x in the $Ge_{1-x}Sn_x$ QDs. 40 nm thick Si capping layers formed on 9 nm diameter (8 ML) $Ge_{1-x}Sn_x$ QDs with values for x of 0, 0.07, 0.15, 0.25, and 0.5. To distinguish between the alloying effect and Sn segregation effect, we also formed 6.8 ML Ge QDs and then deposited 1.2 ML Sn at 200°C. These separately-deposition (SD) dots were covered with 40 nm Si capping layers. For these SD samples, the deposition amount was the same (8 ML) and the ratio of Ge and Sn deposition amounts was 0.85 to 0.15. At small x of 0 to 0.15, RHEED patterns were streaky as shown in Fig. 12(b), indicating that Si capping layers were flat. At x=0.25, the RHEED pattern in Fig. 14(a) shows obscure 1/4 spots indicated by lines in addition to streaky Si diffraction patterns. The 1/4 spots are considered to come from the c(4×4) Sn-absorbed Si(001) surfaces (Baski et al., 1991; Lyman & Bedzyk, 1997), revealing that a small number of Sn atoms segregated to the surface during the formation of the Si capping layer. Both the QD samples with x = 0.5 and the SD samples show spotty RHEED patterns for the Si capping layers as shown in Fig. 14(b) indicating rough surface of Si capping layer. In the samples including the QDs with large x = 0.5 and the SDs, Sn segregation was presumably caused because these samples had large Sn concentrations at the interfaces between QDs and Si capping layers. PL spectra of these Si-capped QDs were measured as shown in Fig. 14(c). The integrated PL peak intensity in the range of 0.75–1.0 eV is also shown in Fig. 14(d). These results reveal that the integrated PL peak intensity has a maximum near x=0.25. The SD samples show the lower PL intensity (open circles) compared with that of the $Ge_{0.85}Sn_{0.15}$ QD sample with the same Sn content x.

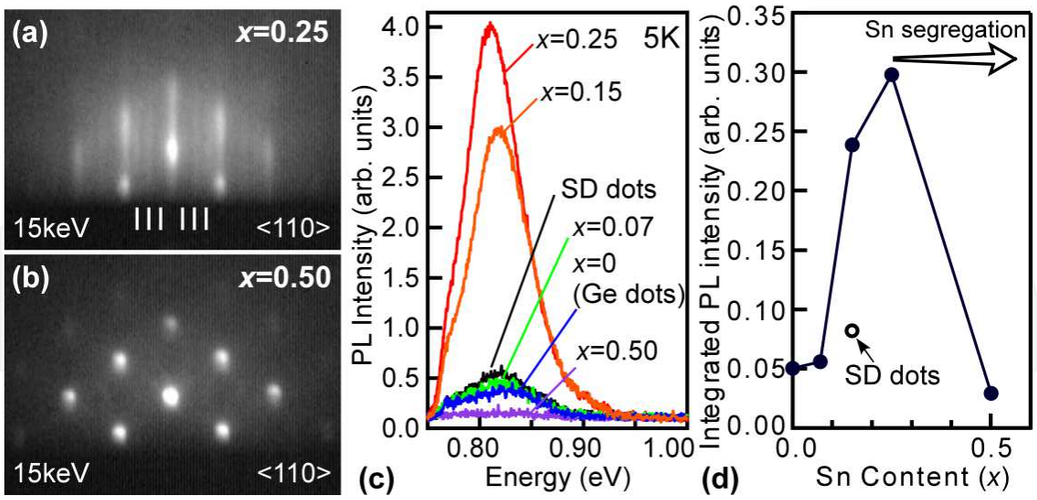

Fig. 14. (a), (b) RHEED pattern of Si/$Ge_{1-x}Sn_x$ QDs/Si(001) structures with x of 0.25 (a) and 0.5 (b). (c) PL spectra of Si/$Ge_{1-x}Sn_x$ QDs/Si(001) structures with various x. (d) Dependence of integrated PL intensity on Sn content x.

We investigated the temperature dependence of the PL peak intensity and PL spectrum as show in Fig. 15. The PL intensity in Fig. 15 bgan to decrease at a temperature higher than 40 K. The integrated PL peak intensity was fitted with $a/(1+b\exp(-E_a/kT))$, where E_a is an activation energy for thermal quenching of the PL, a and b are coefficients, k is the Boltzmann constant, and T is the measurement temperature. As a result, E_a was adjusted to ~22 meV, which is similar to that for the Si-capped Ge QD structures (Ichikawa et al., 2008).

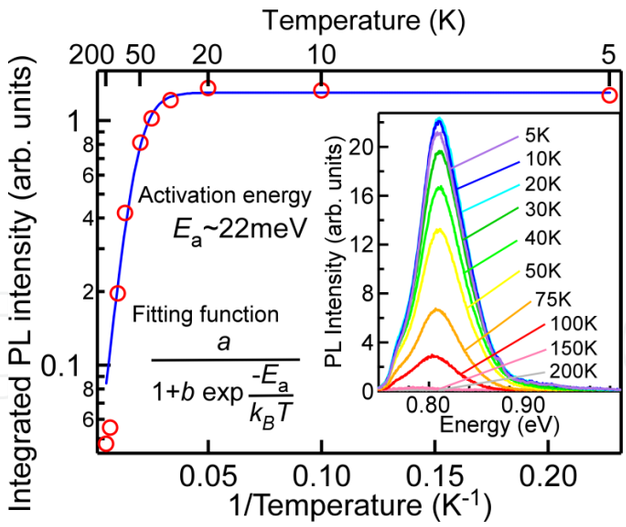

Fig. 15. Measurement temperature dependence of integrated PL intensity of Si/$Ge_{0.85}Sn_{0.15}$ QDs/Si(001) structure. PL spectra was shown in inset.

The PL intensity in the present structures is about ten times higher than that of as-grown Si-capped Ge QD structures. The only difference is the existence of Sn atoms. There are two possible effects: Sn segregation and the Ge-Sn alloying effect. Sn segregation could enhance the formation of the radiative electronic states or remove non-radiative recombination

defects. However, in both the $Ge_{0.5}Sn_{0.5}$ QD sample and the SD sample where Sn atoms segregated into the Si capping layer, the PL intensity reduced as shown in Fig. 14(c). This indicates Sn segregation introduces non-radiative recombination defect centers rather than enhancing the PL intensity. On the other hand, Ge-Sn alloying results in a lattice mismatch between the QDs and Si capping layer larger than that for Ge QDs. In the case of Si-capped Ge QDs, high-temperature-post-annealing can cause the relaxation of strain between Si capping layers and Ge, which plays a role in the formation of radiative electronic states in Si capping layers (Shklyaev et al., 2006). When we adopt this strain-driven formation mechanism of the radiative electronic states, the enhancement of PL intensity can be explained by larger strain in Si-capped $Ge_{1-x}Sn_x$ QDs. At smaller $x<0.25$, where Sn segregation was negligible (Nakamura et al., 2007c), the PL intensity increased monotonically with an increase in x; that is, an increase in the lattice mismatch. This experimental result supports our proposed mechanism: GeSn QDs work as nanometer-size-controlled stressors to introduce radiative electronic states in Si capping layers. Also, the consistencey of the activation energy for thermal quenching between Ge and GeSn QD samples can be reasonable in this model of radiative electronic states in Si capping layer. In the case of Si bulk with radiative defects formed by other techniques such as long-duration or high-temperature-annealing, the PL intensity was reported to be enhanced by introducing strain (Kveder et al.,1995; Leoni et al., 2004). Although the origin of radiative electronic states is still open to question, the strain-driven formation of the radiative electronic states in the Si layer is a plausible mechanism for the enhancement of PL intensity in the present samples.

3.5 Optical properties of modified structures

We investigated hydrogen-plasma treatment effect on PL spectra of $Si/Ge_{1-x}Sn_x$ QDs/Si(001) structures because non-radiative recombination centers can be terminated by hydrogen atoms in general. First, we measured PL spectra of Si/Ge QDs/Si(001) structure (the case of $x=0$) as shown in Fig.16. Hydrogen-plasma treatment was performed at 280°C. This result revealed shape and position of PL peaks were changed by hydrogen-plasma treatment. This demonstrated that the hydrogen-plasma treatment affected the radiative electronic states in Si capping layer. Although the origin of this change is not elucidated yet, there is a possilbity of enhancing the light emitting efficiency and improving thermal properties of Si/GeSn QDs/Si structures by optimizing the treatment condition.

Next, to change barrier materials, we fabricated SiO_2/GeSn QDs/Si sturctures. SiO_2 capping layers of ~70 nm in thickness were formed by Si deposition at the O_2 partial pressure of 2×10^{-4} Pa as shown by RHEED pattern in Fig.17. First 7 nm SiO_2 layer was formed at RT followd by formation of 63 nm SiO_2 layers at 400°C.

We measured PL of SiO_2/8-ML $Ge_{0.85}Sn_{0.15}$ QDs/Si(001) at 5K. There is no PL signal in 0.8 eV range. In order to improve quality of SiO_2, rapid thermal annealing at 800°C for 5 s was peformed, PL of which smaple is shown in Fig. 18(a). The Broad peak was observed in the range of 0.8-1.0 eV. However, sharp structure in PL spectra did not appear. We also measured PL spectra of this sample in visible region as shown in Fig. 18 (b). The strong visible PL was observed, which can be related to the defects in SiO_2 layer. This PL peak has strong light emitting efficency even at RT. Therefore, there is a possibility that 0.8 eV PL was weakend due to the existnece of the defects in SiO_2 causing visible PL with high light emitting efficiency. This indicates that there is a room of developing SiO_2/GeSn QDs/Si structures with high light emitting efficiency near 0.8 eV by improving SiO_2 capping layer.

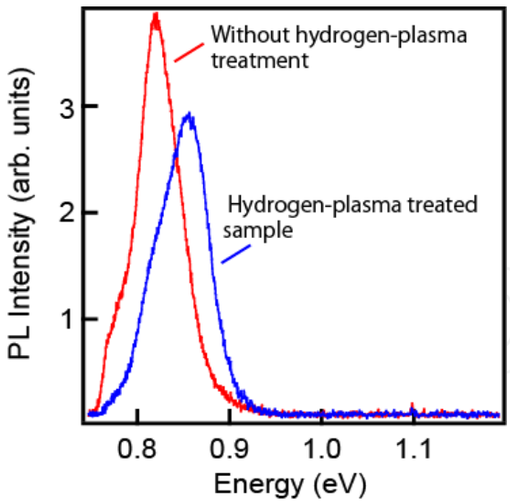

Fig. 16. PL spectra of Si/Ge QDs/Si(001) structures with and without hydrogen-plasma treatment.

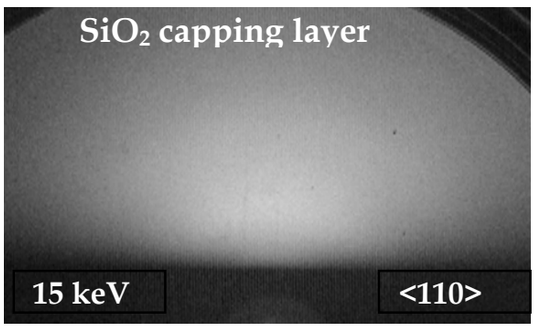

Fig. 17. RHEED pattern of SiO_2 layer formed on 8-ML $Ge_{0.85}Sn_{0.15}$ QDs/Si(001)

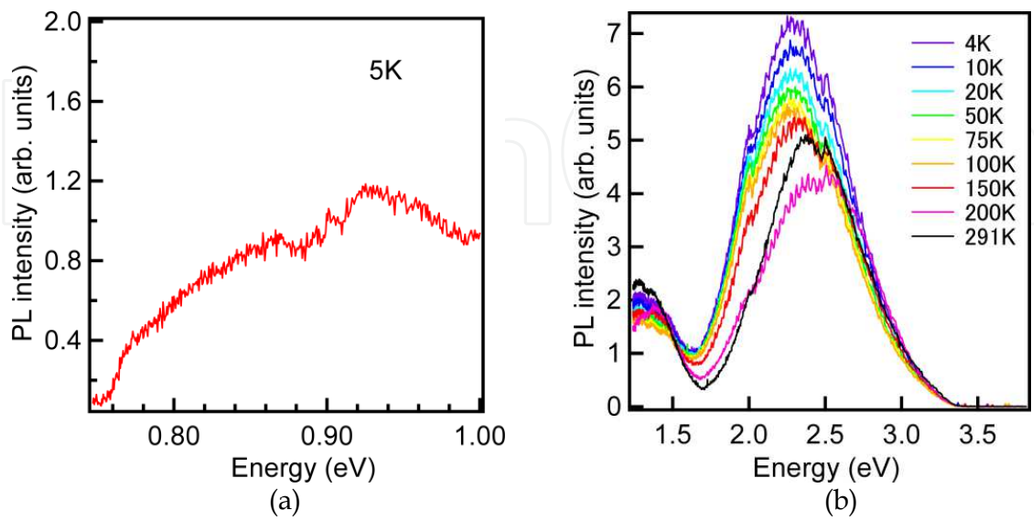

Fig. 18. PL spectra arounnd 0.9 (a) and 2 eV (b) of SiO_2/8-ML $Ge_{0.85}Sn_{0.15}$ QDs/Si(001) structure.

4. Conclusion

We developed the epitaxial growth technique of ultrahigh density GeSn QDs on Si substrates using the ultrathin SiO_2 films. For the epitaxial growth , nanowindows were formed on the ultrathin SiO_2 films by predeposition of 2-ML Ge at 650°C, which condition is key factor. Annealing at 500°C for 3 min improved low crystallinity of low-temperature-grown QDs, which did not cause Sn segregation. The GeSn QDs exhibited the quantum confinement effect which was observed by STS. STS results revealed that the peak width of the quantum levels in QDs depended on the QD shape, which can be explained by electronic state change from the quasi-0-dimensional to quasi-2-dimensional ones. Strong PL was observed in Si/GeSn QDs/Si near 0.8 eV. This origin can be related to radiative electronic states in Si capping layer, which formation strongly depended on the strain-states near the interfaces between QDs and Si capping layers. The radiative electronic states can be changed by hydrogen-plasma treatment. From SiO_2-capped GeSn QDs, featureless PL appeared at around 0.8 eV. Strong visible PL was also observed even at RT which is related to SiO_2 defects. These results indicate material design based on GeSn QDs/Si structures exhibites a possiblity to develop the Si-based light emitting materials near 0.8 eV with high efficiency.

5. Acknowledgment

We thank Prof. N. Tanaka, and Dr. S. P. Cho for TEM and STEM observation.

6. References

Baski, A. A.; Quate, C. F. & Nogami, J. (1991). Tin-induced reconstructions of the Si(100) surface. *Phys. Rev. B*, 44, 11167-11177

Boland, J.J. (1991). Evidence of pairing and its role in the recombinative desorption of hydrogen from the Si(100)-2 x 1 surface. *Phys. Rev. Lett.*, 67, 1539-1542

Cullis, A. G. & Canham, L. T. (1991). Visible light emission due to quantum size effects in highly porous crystalline silicon. *Nature*, 353 335-338

de Guevara, H. P. L., Rodríguez, A. G., Navarro-Contreras, H. & Vidal M. A. (2003). $Ge_{1-x}Sn_x$ alloys pseudomorphically grown on Ge(001). *Appl. Phys. Lett.*, 83, 4942-4944

de Guevara, H. P. L.; Rodríguez, A. G.; Navarro-Contreras, H. &Vidal M. A. (2004). Determination of the optical energy gap of $Ge_{1-x}Sn_x$ alloys with $0<x<0.14$. *Appl. Phys. Lett.*, 84, 4532-4534

Eaglesham, D. J. & Cerullo, M. (1990). Dislocation-free Stranski-Krastanow growth of Ge on Si(100). *Phys. Rev. Lett.* 64, 1943-1946

Grandidier B. (2004). Scanning tunnelling spectroscopy of low-dimensional semiconductor systems. *J. Phys.: Condens. Matter*, 16, S161-S170

Gurdal, O.; Desjardins, P.; Carlsson, J. R. A.; Taylor, N.; Radamson, H. H.; Sundgren, J.E. & Greene, J. E. (1998). Low-temperature growth and critical epitaxial thicknesses of fully strained metastable $Ge_{1-x}Sn_x$ ($x \leq 0.26$) alloys on Ge(001) 2×1. *J. Appl. Phys.*, 83, 162-170

He, G. & Atwater H. A. (1997). Interband Transitions in Sn_xGe_{1-x} Alloys. *Phys. Rev. Lett.*, 79, 1937-1940

Ichikawa, M.; Uchida S.; Shklyaev A. A.; Nakamura Y.; Cho S. P. & Tanaka N. (2008). Characterization of semiconductor nanostructures formed by using ultrathin Si oxide technology. Appl. Surf. Sci. 255, 669-671

Jenkins, D. W. & Dow, J. D. (1987). Electronic properties of metastable Ge_xSn_{1-x} alloys. *Phys. Rev. B*, 36, 7994-8000

Kveder, V. V.; Steinman, E. A.; Shevchenko, S. A. & Grimmeiss H. G. (1995). Dislocation-related electroluminescence at room temperature in plastically deformed silicon. *Phys. Rev. B*, 51, 10520-10526

Leoni E.; Binetti, S.; Pichaud, B. & Pizzini S. (2004). Dislocation luminescence in plastically deformed silicon crystals: effect of dislocation intersection and oxygen decoration. *Eur. Phys. J. Appl. Phys.*, 27, 123–127

Lyman, P. F. & Bedzyk, M. J. (1997). Local structure of Sn/Si(001) surface phases. *Surf. Sci.*, 371, 307-315

Maeda, Y. (1995). Visible photoluminescence from nanocrystallite Ge embedded in a glassy $Si0_2$ matrix: Evidence in support of the quantum-confinement mechanism. *Phys. Rev. B*, 51, 1658-1670

Nakamura, Y.; Mera, Y. & Maeda, K. (1999). A reproducible method to fabricate atomically sharp tips for scanning tunneling microscopy. *Rev. Sci. Instrum.*, 70, 3373-3376

Nakamura, Y.; Nagadomi, Y.; Sugie, K.; Miyata, N. & Ichikawa, M. (2004). Formation of ultrahigh density Ge nanodots on oxidized Ge/Si(111) surfaces. *J. Appl. Phys.*, 95, 5014-5018

Nakamura, Y.; Watanabe, K.; Fukuzawa, Y. & Ichikawa, M. (2005). Observation of the quantum-confinement effect in individual Ge nanocrystals on oxidized Si substrates using scanning tunneling spectroscopy. *Appl. Phys. Lett.*, 87, 133119-1-3

Nakamura, Y.; Nagadomi, Y. Cho, S. P.; Tanaka, N. & Ichikawa, M. (2006). Formation of ultrahigh density and ultrasmall coherent β-$FeSi_2$ nanodots on Si(111) substrates using Si and Fe codeposition method. *J. Appl. Phys.*, 100, 044313-1-5

Nakamura, Y.; Ichikawa, M.; Watanabe, K. & Hatsugai, Y. (2007a). Quantum fluctuation of tunneling current in individual Ge quantum dots induced by a single-electron transfer. *Appl. Phys. Lett.*, 90, 153104-1-3

Nakamura, Y.; Masada, A. & Ichikawa, M. (2007b). Quantum-confinement effect in individual $Ge_{1-x}Sn_x$ quantum dots on Si(111) substrates covered with ultrathin SiO_2 films using scanning tunneling spectroscopy. *Appl. Phys. Lett.*, 91, 013109-1-3

Nakamura, Y.; Masada A.; Cho, S. P.; Tanaka, N. & Ichikawa M. (2007c). Epitaxial growth of ultrahigh density $Ge_{1-x}Sn_x$ quantum dots on Si(111) substrates by codeposition of Ge and Sn on ultrathin SiO_2 films. *J. Appl. Phys.*, 102, 124302-1-6

Nakamura, Y.; Sugimoto, T. & Ichikawa, M. (2009). Formation and optical properties of GaSb quantum dots epitaxially grown on Si substrates using an ultrathin SiO_2 film technique. *J. Appl. Phys.*, 105, 014308-1-4

Nakamura, Y.; Murayama A.; Watanabe R.; Iyoda T. & Ichikawa M. (2010). Self-organized formation and self-repair of a two-dimensional nanoarray of Ge quantum dots epitaxially grown on ultrathin SiO_2-covered Si substrates. *Nanotechnology*, 21, 095305-1-5

Nakamura, Y.; Miwa, T. & Ichikawa, M. (2011a). Nanocontact heteroepitaxy of thin GaSb and AlGaSb films on Si substrates using ultrahigh-density nanodot seeds. *Nanotechnology* 22, 265301-1-7

Nakamura, Y.; Murayama, A. & Ichikawa, M. (2011b). Epitaxial Growth of High Quality Ge Films on Si(001) Substrates by Nanocontact Epitaxy. *Cryst. Growth Des.*, 11, 3301-3305

Niquet, Y. M.; Allan, G.; Delerue, C. & Lannoo M. (2000). Quantum confinement in germanium nanocrystals. *Appl. Phys. Lett.*, 77, 1182-1184

Ragan, R. & Atwater, H. A. (2000). Measurement of the direct energy gap of coherently strained Sn_xGe_{1-x}/Ge(001) heterostructures. *Appl. Phys. Lett.*, 77, 3418-3420.

Schmidt, O. G. & Eberl, K. (2000). Multiple layers of self-asssembled Ge/Si islands: Photoluminescence, strain fields, material interdiffusion, and island formation. *Phys. Rev. B*, 61, 13721-13729,

Shklyaev, A. A.; Shibata, M. & Ichikawa, M. (2000). High-density ultrasmall epitaxial Ge islands on Si(111) surfaces with a SiO_2 coverage. *Phys. Rev. B*, 62, 1540-1543

Shklyaev, A. A. & Ichikawa, M. (2002). Three-dimensional Si islands on Si(001) surfaces. *Phys. Rev. B*, 65, 045307-1-6

Shklyaev, A. A.; Nobuki, S.; Uchida, S.; Nakamura, Y. & Ichikawa, M. (2006). Photoluminescence of Ge/Si structures grown on oxidized Si surfaces. *Appl. Phys. Lett.*, 88 121919-1-3

Shklyaev, A. A.; Cho, S. P.; Nakamura, Y., Tanaka, N. & Ichikawa, M. (2007). Influence of growth and annealing conditions on photoluminescence of Ge/Si layers grown on oxidized Si surfaces. *J. Phys.: Condens. Matter*, 19, 136004-1-8

Matsudo, T.; Ohta T.; Yasuda, T.; Nishizawa M.; Miyata N.; Yamasaki S.; Shklyaev, A. A. & Ichikawa M. (2002). Observation of oscillating behavior in the reflectance difference spectra of oxidized Si(001) surfaces. *J. Appl. Phys.*, 91, 3637-3643

Wolkin, M. V.; Jorne, J.; Fauchet,P. M.; Allan, G. & Delerue, C. (1999). Electronic States and Luminescence in Porous Silicon Quantum Dots: The Role of Oxygen. *Phys. Rev. Lett.*, 82, 197-200

State-of-the-Art of Quantum Dot System Fabrications

Edited by Dr. Ameenah Al-Ahmadi

ISBN 978-953-51-0649-4
Hard cover, 172 pages
Publisher InTech
Published online 13, June, 2012
Published in print edition June, 2012

The book "State-of-the-art of Quantum Dot System Fabrications" contains ten chapters and devotes to some of quantum dot system fabrication methods that considered the dependence of shape, size and composition parameters on growth methods and conditions such as temperature, strain and deposition rates. This is a collaborative book sharing and providing fundamental research such as the one conducted in Physics, Chemistry, Material Science, with a base text that could serve as a reference in research by presenting up-to-date research work on the field of quantum dot systems.

How to reference

In order to correctly reference this scholarly work, feel free to copy and paste the following:

Yoshiaki Nakamura and Masakazu Ichikawa (2012). Formation of Ultrahigh Density Quantum Dots Epitaxially Grown on Si Substrates Using Ultrathin SiO2 Film Technique, State-of-the-Art of Quantum Dot System Fabrications, Dr. Ameenah Al-Ahmadi (Ed.), ISBN: 978-953-51-0649-4, InTech, Available from: http://www.intechopen.com/books/state-of-the-art-of-quantum-dot-system-fabrications/formation-of-ultrahigh-density-quantum-dots-epitaxially-grown-on-si-substrates-using-ultrathin-s

INTECH
open science | open minds

InTech Europe
University Campus STeP Ri
Slavka Krautzeka 83/A
51000 Rijeka, Croatia
Phone: +385 (51) 770 447
Fax: +385 (51) 686 166
www.intechopen.com

InTech China
Unit 405, Office Block, Hotel Equatorial Shanghai
No.65, Yan An Road (West), Shanghai, 200040, China
中国上海市延安西路65号上海国际贵都大饭店办公楼405单元
Phone: +86-21-62489820
Fax: +86-21-62489821

IntechOpen